

Torque and Bearing Reaction Forces Simulation of Micro-Magnetic Gears

M. Muñoz-Martínez¹, E. Diez-Jimenez¹, M. J. Gómez-García², R. Rizzo³, and A. Musolino³

¹Mechanical Engineering Area, Universidad de Alcalá, Spain
miriam.martinezm@uah.es, efren.diez@uah.es

²Mechanical Engineering Department, Universidad Carlos III de Madrid, Spain
mjggarci@ing.uc3m.es

³Department of Energy and Systems Engineering, University of Pisa, Largo Lucio Lazzarino, 56122, Pisa, Italy
rocco.rizzo@unipi.it, antonino.musolino@unipi.it

Abstract — Specific torque and bearing reaction forces are simulated for two models of axial flux magnetic gears. The models cover simulation in two scale ranges: hundreds of microns and tenths of microns. The simulations presented are performed considering currently available magnetic properties in the microscale and potentially achievable ones. Specific torque of the models is between 2.76 up to 8.24 Nm/kg. This range is large enough to overpass conventional toothed microgear specific torque. This means that micro magnetic gears can not only provide conversion of speed and torque without friction but also to be more compact.

Index Terms — Axial flux rotary machines, FEM simulation, magnetic gear, microgears, micromagnets.

I. INTRODUCTION

MEMS (MicroElectroMechanical Systems) contain moving parts that are susceptible to friction, wear and fatigue. Friction and wear are undesired phenomena in machines because they reduce their efficiency and lifetime. In the microscale, friction and wear are primarily imposed by surface forces (capillary, van der Waals, electrostatic, or frictional forces) and surface parameters (i.e., surface roughness or adhesion) [1]–[3].

In the macroscale, friction forces are much lower than inertial ones, thus lubrication is good enough to keep a high efficiency and long lifetime of mechanisms. Nevertheless, when the size is reduced, friction forces become more important and the efficiency decreases dramatically. Many MEMS are impossible or impractical to protect from external contamination. Thus, not only water vapour but also other contaminants chemically interact and stick. Friction and wear are the most crucial phenomena that finally determine the reliability of MEMS [4]–[6].

Wear and friction in MEMS depend on size, surface roughness, coatings and lubricants. Previous research

works have studied these effects explaining the differences in tribological aspects from micro to nanoscale [7], [8]. Although the results of these studies show interesting enhancements, friction and wear is unavoidable since contact forces always appear.

Magnetomechanical components can be a good choice in order to reduce or even completely avoid wear in MEMS. Any kind of mechanism is susceptible of conversion to its magneto-mechanical equivalent. Spur gears [9], planetary gears [10], harmonic-drives [11]–[13] couplings [14], bevel gear, cycloidal gear, can be converted to its magnetic equivalent. Not only gears can be converted but also bearings, springs [15]–[17], suspensions and even structures can be created.

These types of components have already been tested in macroscale [18]–[22] preventing from wear and friction in the teeth transmission or in the bearings. Even more, they have been combined (bearings, gear and coupling) as demonstrated in the first fully contactless machine ever built [23]. All these components are completely passive; they behave as conventional mechanical elements but with additional advantages.

All the benefits of magneto-mechanical components are inherent to the lack of contact. Nevertheless, the main pitfall for their wide adoption in the macroscale has always been their lower specific capacity for torque/force transmission with respect to conventional ones [24]. For magneto-mechanical components, the transmitted force/torque, in first term, depends directly on the amount of magnetic material in the mechanism. This implies that the specific force/torque (Nm/kg) remains constant for any scale. On the contrary, for conventional mechanical elements the miniaturization increases friction/inertial force ratio, thus specific force/torque decreases when reducing size. This effect permits to establish a frontier wherein micromagnetic gears also would perform better in terms of specific torque. This frontier has been set in 2 mm characteristic diameter with currently available

magnetic material properties and around 9 mm diameter if best magnetic material properties were achieved [25].

In this work, the specific torque and bearing reaction forces are simulated for two models of axial flux magnetic gears. The models cover simulation in two scale ranges: hundreds of microns and tenths of microns. The simulations presented are performed considering currently available magnetic properties in the microscale and potentially achievable ones.

II. PERMANENT MAGNETS FOR MEMS

The fabrication of high-quality permanent magnets with size in the 1-1000 μm range is still very challenging. Permanent Magnets are essential components for MEMS devices such as motors, generators, pumps, sensors, acoustic speakers and others. After magnetization, PM provide “free” constant source of magnetic fields, requiring no external power. PM are often coupled with soft magnetic cores to guide and concentrate the fields in certain regions as for example in magnetic gears

Current micromanufacturing techniques for PM are divided into deposited micromagnets (from 0.5 to 50 μm thickness) and powder micromagnets (from 10 μm to 1 mm thickness). Deposition of micromagnets includes physical vapour deposition (sputtering, evaporation and pulse-laser deposition) [27]. Since high magnetic product rare earth micromagnets cannot be electroplated from aqueous baths, the available techniques for deposition are sputtering and PLD [28].

Using powder techniques as sintering or bonding PM can be done in the range of 10 μm to 1 mm. With this method, powders size determine the minimum PM size. Likewise for macroscale PM, bonded micro-magnets properties are usually weaker than those of the original magnetic powder. The coercivity remains constant but the remanence is directly related to the particle fill factor, reaching at best 80%. The values obtained even in the best solution found in literature are low (for NdFeB not larger than remanence 0.7 T and remanence 1090 kA/m, separately). Table 1 summarizes methods, thickness and highest magnetic properties of micro permanent magnets [29].

Table 1: NdFeB Permanent Magnets properties for different micro-manufacturing techniques

Method	E (μm)	Br (T)	Hc (kA/m)	BH _{mx} (kJ/m ³)	Assem.
Deposition	0.5-50	0.5-1.4	600-1035	150-400	Integral
Powder	50-1000	0.2 – 0.7	300-800	14-250	Integral
Bulk $\mu\text{machining}$	25-1000	1 – 1.4	860-1035	342-406	Manual Brittle
Macroscale	>1000	1 – 1.4	860-1035	342-406	Manual

III. MICRO-MAGNETIC GEAR DESIGN

Axial flux micro-magnetic gear topology is chosen because it has demonstrated high specific torque

performance in the macroscale and because its stack type topology is very adequate to typical epitaxial MEMS fabrication processes.

The magnetic gear design consists of an input or fast rotary element made by several PM, an intermediate element, typically static, made of soft magnetic material and a third element acting as output or slow rotary element made again of a set of PM.

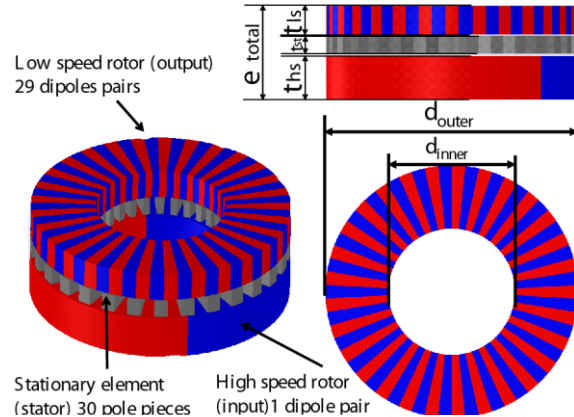


Fig. 1. Micro-magnetic gear geometrical parameters.

The permanent magnet arrangement is done in alternative polarizations, (red and blue in Fig. 1). All the polarizations of the PM are oriented towards the vertical direction (blue-north pole, red-south pole). The number of dipole-pairs in low speed rotor is $N_{\text{output}}=29$; the number of stationary steel pole-pieces is $N_{\text{stator}}=30$; and the number of dipole-pairs in high-speed rotor is $N_{\text{input}}=1$. Gear ratio (G_r) is given by the relationship between the different elements. It is calculated as:

$$G_r = \frac{N_{\text{output}} - N_{\text{stator}}}{N_{\text{output}}} \quad (1)$$

This expression is valid if the number of dipole pairs in the input is equal to the difference between N_{output} and N_{stator} , i.e., $N_{\text{stator}}=1$. In this case, $G_r = -1/29$. Bearings, axles and frames will contribute with extra weight. Therefore, it is necessary to estimate final corrected specific torque values. Considering previous magnetic gear developments, a correction factor of 1.1 is reasonable for the final device weight [22], [30].

Two ranges of application are explored: hundreds of microns and tenths of microns. Thus, two different models have been created. The geometrical parameters of each model are listed in Table 2.

Vacoflux 48 ($B_{\text{sat}}=2.35$ T) is considered as soft magnetic material of the stator and NdFeB material for the two rotors. As already mentioned, the simulations presented are performed considering currently available magnetic properties in the microscale ones and potentially achievable ones. Available selection of properties depends on thickness of the rotor. Permanent magnetic material properties used are listed in Table 3.

Table 2: Geometrical parameters of the magnetic gears

Definition	Sym.	Model 1 (Submilimetric)	Model 2 (Micrometric)
Outer diameter (μm)	d_{outer}	700	140
Inner diameter (μm)	d_{inner}	350	70
Total length (μm)	e_{total}	260	52
Low speed rotor thickness (μm)	t_{ls}	80	16
Stator thickness (μm)	t_{st}	50	10
High speed rotor thickness (μm)	t_{hs}	120	24
Airgap Low Speed roto-Stator (μm)	$g_{\text{ls-st}}$	4	0.8
Airgap Stator-High Speed rotor (μm)	$g_{\text{st-hs}}$	6	1.2
Magnetic parts weight (mg)	W_{mag}	0.5478	0.0044
Estimated weight (mg)	W_{tot}	0.6028	0.0048

Table 3: Magnetic material properties

Material Name	Br (T)	Hc (kA/m)
NdFeB ideal	1.42	1035
NdFeB real thin film (< 50 μm)	1.3	955
NdFeB real submilimetric	0.7	800
Vacoflux 48	1.5	0.150

IV. FEM MODEL AND SIMULATIONS

All the calculations are done using a finite element model (FEM) software for electromagnetic fields. The solver chosen is the magneto-static solver. The magneto-static field solution verifies the following two Maxwell's equations:

$$\nabla \times \vec{H} = \vec{J} \text{ and } \nabla \cdot \vec{B} = 0.$$

With the following relationship at each material:

$$\vec{B} = \mu_0(\vec{H} + \vec{M}) = \mu_0 \cdot \mu_r \cdot \vec{H} + \mu_0 \cdot \vec{M}_p. \quad (2)$$

Where H is the magnetic field intensity, B is the magnetic field density, J is the conduction current density, M_p is the permanent magnetization, μ_0 is the permeability of vacuum and μ_r is the relative permeability [31].

The geometrical 3D model is shown in Fig. 2. In this model, the angular position of the low speed rotor can be automatically modified by the software at each simulation. The mesh of the model is more refined in the magnetic material interfaces and also within the airgaps. An example of the mesh is also shown in Fig. 2.

The materials considered are dependent on the thickness of the rotor. The combination of models and materials leads to four parametric magneto-static simulations. The summary of the simulations and

materials selected for each element is given in Table 4.

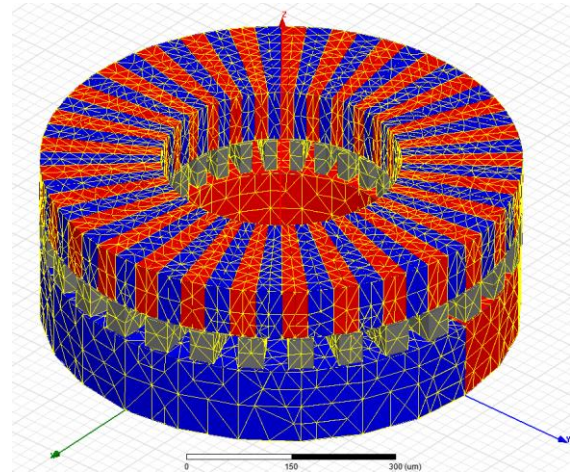


Fig. 2. 3D view of the FEM model: geometry and mesh.

Table 4: Simulation list

N°	Model	Low Speed Rotor Material	High Speed Rotor Material	Stator Material
1R	Model 1	NdFeB real submilimetric	NdFeB real submilimetric	Vacoflux 48
1I	Model 1	NdFeB ideal	NdFeB ideal	Vacoflux 48
2R	Model 2	NdFeB real thin film	NdFeB real thin film	Vacoflux 48
2I	Model 2	NdFeB ideal	NdFeB ideal	Vacoflux 48

As boundary conditions a “Zero tangential Field” type condition is applied in the external surfaces of the surrounding region volume. No current or field excitation is used, only permanent magnetization excitation according to the material properties table.

Each simulation corresponds to a single combination of the model and material properties. Forces and torques are obtained in post-processing by using the virtual forces principle. The output and input torque and corresponding reaction forces at each element are calculated for every angular position. Each simulation has been done considering a stationary condition.

The solver uses an adaptive meshing solver. Typically 11-13 iterations on the mesh are sufficient for a correct convergence of the simulation. The total number of tetrahedral elements is around 200000. The mesh is refined for achieving less than 2% of energy error within a simulation time of less than 20 seconds per simulation. All the simulations have been done in a workstation with an Intel Core i4-4690 with 8Gb of RAM memory.

The selection of this computational working point has been chosen after performing a sensitivity analysis of the FEM results, Fig. 3. In this figure, it is shown that error highly decreases from more than 150000 elements while computational time is still low.

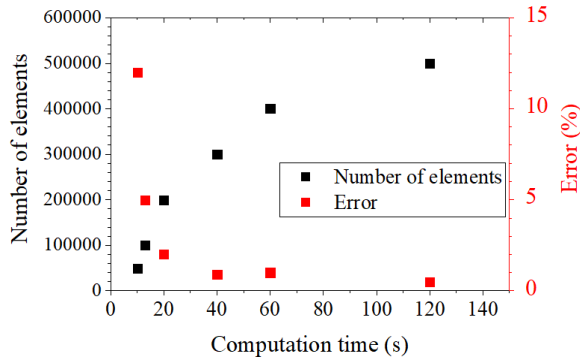


Fig. 3. Number of elements sensitivity analysis.

V. RESULTS AND DISCUSSION

The results present, in next figures, torques and axial forces for each model as a function of the rotation angle of the corresponding input rotor. The radial forces are negligible due to the axial geometry of the gear.

Figure 4 shows torques of input and output rotor of model 1 for both material combination 1R and 1I with respect to the angle of rotation of the input rotor. The maximum output torque is achieved at 90 degrees for both combinations, in agreement with the topology of the gear. The maximum output torque for the real material combination is 1.66 μNm and the one for the ideal material combination is 4.95 μNm . The torque in the input rotor is 29 times smaller than the one in the output as expected.

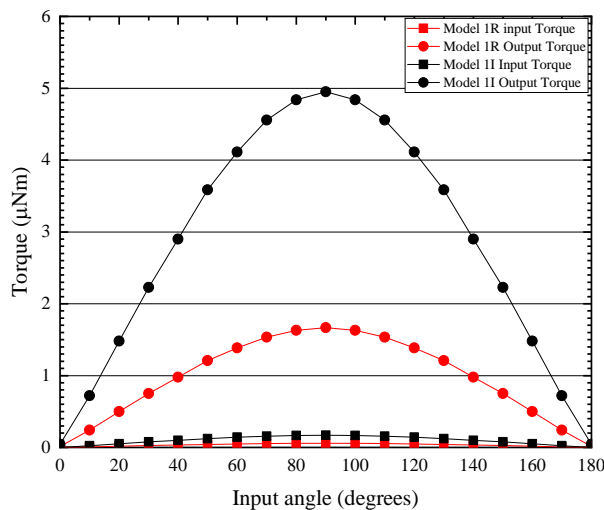


Fig. 4. Torques for Model 1R and 1I.

Figure 5 shows the axial forces acting on input and output rotor of model 1 for both material combination 1R and 1I with respect to the angle of rotation of the input rotor. The maximum axial force is 63.22 mN achieved at 0 degrees of input rotation in the output element corresponding to the ideal materials case. The maximum axial force for the real material case is 18.75 mN obtained also at 0 degrees of rotation of the input rotor.

Figure 6 shows torques of input and output rotor of model 2 for both material combination 2R and 2I with respect to the angle of rotation of the input rotor. The maximum output torque is achieved at 90 degrees for both combinations, in agreement with the topology of the gear. The maximum output torque for the real material combination is 0.0331 μNm and the one for the ideal material combination is 0.0397 μNm . The torque in the input rotor is 29 times smaller than the one in the output.

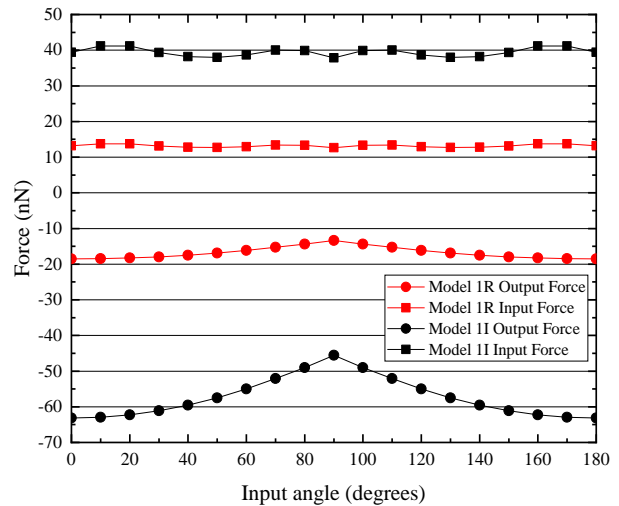


Fig. 5. Axial forces for Model 1R and 1I.

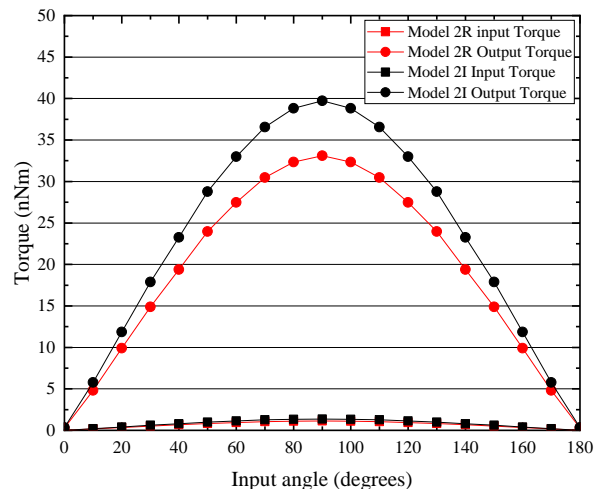


Fig. 6. Torques for Model 2R and 2I.

Figure 7 shows the axial forces acting on input and output rotor of model 2 for both material combination 2R and 2I with respect to the angle of rotation of the input rotor. The maximum axial force is 2.11 mN achieved at 0 degrees of input rotation in the output element corresponding to the ideal materials case. The maximum axial force for the real material case is 2.10 mN obtained also at 0 degrees of input rotation.

Specific torque of the models is between 2.76 up to 8.24 Nm/kg. This range is large enough to overpass conventional toothed microgear specific torque [25]. This means that micro magnetic gears can not only provide conversion of speed and torque without friction but also be more compact. It is important to notice that specific torque for both ideal models is almost equal for both sizes, demonstrating that specific torque is independent of the order of magnitude of the size. A summary of the results is presented in Table 5.

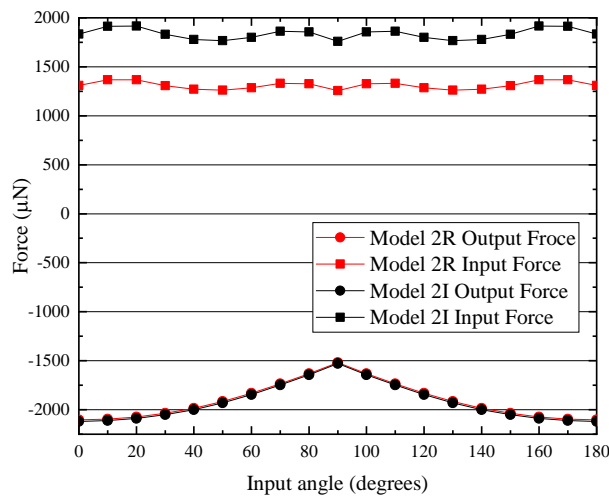


Fig. 7. Axial forces for Model 2R and 2I.

Table 5: Results summary

Model	Output Torque Max. (μNm)	Axial Force Max. (mN)	Specific Torque (Nm/kg)
Model 1 Real	1.66	18.75	2.76
Model 1 Ideal	4.95	63.22	8.21
Model 2 Real	0.0331	2.10	6.86
Model 2 Ideal	0.0397	2.11	8.24

For model 1 the difference between the model with ideal material and with real material is significant. The maximum output torque in the ideal materials model is 2.98 times larger than with real materials properties, so it happens with the specific torque and axial force. Thus, it can be interesting for science material researchers to keep on working on enhancement of NdFeB properties for magnets in the submillimetric range. For model 2

the difference between the model with ideal material and with real material is smaller, just a 1.2. Therefore, micromagnetic gears in the micrometric range would have an outstanding specific torque capacity. Hence, it can be interesting to develop manufacturing systems for such devices.

VI. CONCLUSION

MEMS contain moving parts that are susceptible to friction, wear and fatigue. Friction and wear are undesired phenomena in machines because they reduce their efficiency and lifetime. Magnetic gears can be a good choice in order to reduce wear in MEMS since they transmit torques without contact.

In this work, the specific torque and bearing reaction forces are simulated for two models of axial flux magnetic gears. The models cover simulation in two scale ranges: hundreds of microns and tenths of microns. The simulations presented are performed considering currently available magnetic properties in the microscale and potentially achievable ones.

Specific torque of the models is between 2.76 up to 8.24 Nm/kg. This range is large enough to overpass conventional toothed microgear specific torque. This means that not only micro magnetic gears can provide conversion of speed and torque without friction but also that they can be more compact.

ACKNOWLEDGMENT

The research leading to these results has received funding from the Universidad de Alcalá 2017 research programme under Grant No. CCGP2017/EXP-011.

REFERENCES

- [1] G. Subhash, A. D. Corwin, and M. P. de Boer, "Evolution of wear characteristics and frictional behavior in MEMS devices," *Tribol. Lett.*, vol. 41, no. 1, pp. 177-189, Jan. 2011.
- [2] M. Kawano, K. Sahrani, S. Mori, T.; Kuroda, and M. Tentzeris, "Numerical modeling of reconfigurable RF MEMS-based structures involving the combination of electrical and mechanical force," *Appl. Comput. Electromagn. Soc. J.*, vol. 21, no. 1, pp. 1-8, 2006.
- [3] R. Barmada, S. Musolino, and A. Rizzo, "Equivalent network approach for the simulation of MEMS devices," *Appl. Comput. Electromagn. Soc. J.*, vol. 21, no. 1, pp. 16-25, 2006.
- [4] J. Iannacci, "Reliability of MEMS: A perspective on failure mechanisms, improvement solutions and best practices at development level," *Displays*, vol. 37, pp. 62-71, 2015.
- [5] H.-W. Wu, Y.-Y. Chen, and J.-H. Horng, "The analysis of three-body contact temperature under the different third particle size, density, and value of friction," *Micromachines*, vol. 8, no. 10, p. 302,

- Oct. 2017.
- [6] O. Penkov, M. Khadem, A. Nieto, T.-H. Kim, and D.-E. Kim, "Design and construction of a micro-tribotester for precise in-situ wear measurements," *Micromachines*, vol. 8, no. 4, p. 103, Mar. 2017.
- [7] M. Tauviquirrahman, R. Ismail, J. Jamari, and D. J. Schipper, "Friction reduction in lubricated-MEMS with complex slip surface pattern," *Procedia Eng.*, vol. 68, pp. 331-337, 2013.
- [8] R. W. Carpick, E. E. Flater, J. R. VanLangendon, and M. P. De Boer, "Friction in MEMS: From single to multiple asperity contact," *Proc. SEM VIII Int. Congr. Expo. Exp. Appl. Mech.*, p. 282, 2002.
- [9] F. Jorgensen and T. Andersen, "Two dimensional model of a permanent magnet spur gear," *Conf. Rec. 2005 IEEE Ind. Appl. Conf.*, vol. 1-4, pp. 261-265, 2005.
- [10] C.-C. Huang, M.-C. Tsai, D. G. Dorrell, and B.-J. Lin, "Development of a magnetic planetary gearbox," *IEEE Trans. Magn.*, vol. 44, no. 3, pp. 403-412, Mar. 2008.
- [11] B. Majidi and J. Milimonfared, "Design and analysis of an interior continuous magnetic gear box using finite element method," *Appl. Comput. Electromagn. Soc. J.*, vol. 30, no. 1, pp. 109-116, 2015.
- [12] N. Niguchi and K. Hirata, "Cogging torque analysis of magnetic gear," *IEEE Trans. Ind. Electron.*, vol. 59, no. 5, pp. 2189-2197, 2012.
- [13] R. C. Holehouse, K. Atallah, and J. Wang, "A linear magnetic gear," *Proc. - 2012 20th Int. Conf. Electr. Mach. ICEM 2012*, pp. 563-569, 2012.
- [14] Y. D. Yao, D. R. Huang, C. M. Lee, S. J. Wang, D. Y. Chiang, and T. F. Ying, "Magnetic coupling studies between radial magnetic gears," *IEEE Trans. Magn.*, vol. 33, no. 5, pp. 4236-4238, 1997.
- [15] J. Zhang, L. L. Huang, "Stability analysis for a flywheel supported on magnetic bearings with delayed feedback control," *Appl. Comput. Electromagn. Soc. J.*, vol. 32, no. 8, pp. 642-649, 2017.
- [16] R. Muscia, "Magneto-mechanical model of passive magnetic axial bearings versus the eccentricity error - Part I: Physical mathematical model," *Appl. Comput. Electromagn. Soc. J.*, vol. 32, no. 8, pp. 670-677, 2017.
- [17] E. Diez-Jimenez, A. Musolino, R. Rizzo, and E. Tripodi, "Analysis of the static and dynamic behavior of a non hysteretic superconductive passive magnetic linear bearing by using an electromagnetic integral formulation," *Prog. Electromagn. Res. M*, vol. 50, pp. 183-193, 2016.
- [18] E. Diez-Jimenez, J.-L. Perez-Diaz, and J. C. Garcia-Prada, "Local model for magnet-superconductor mechanical interaction: experimental verification," *J. Appl. Phys.*, vol. 109, no. 6, pp. 063901-063901-5, 2011.
- [19] S. A. Afsari, H. Heydari, and B. Dianati, "Cogging torque mitigation in axial flux magnetic gear system based on skew effects using an improved quasi 3-D analytical method," *IEEE Trans. Magn.*, vol. 51, no. 9, pp. 1-11, 2015.
- [20] C. Cristache, E. Diez-Jimenez, I. Valiente-Blanco, J. Sanchez-Garcia-Casarrubios, and J. L. Perez-Diaz, "Aeronautical magnetic torque limiter for passive protection against overloads," *Machines*, vol. 4, no. 3, 2016.
- [21] E. Diez-Jimenez, "Design and analysis of a non-hysteretic passive magnetic linear bearing for cryogenic environments," *Proc. Inst. Mech. Eng. Part J J. Eng. Tribol.*, 2014.
- [22] J. Esnoz-Larraya, *et al.*, "OPTIMAGDTRIVE: High-performance magnetic gears development for space applications," in *ESMATS*, 2017.
- [23] J. L. Perez-Diaz and E. Diez-Jimenez, "Performance of magnetic-superconductor non-contact harmonic drive for cryogenic space applications," *Machines*, vol. 3, no. 3, pp. 138-156, 2015.
- [24] P. In, "Comparison of magnetic-gear permanent magnet machines," *Prog. Electromagn. Res.*, vol. 133, no. 2013, pp. 177-198, 2013.
- [25] E. Diez-Jimenez, R. Sanchez-Montero, and M. Martinez-Muñoz, "Towards miniaturization of magnetic gears: Torque performance assessment," *Micromachines*, vol. 9, no. 1, p. 16, Dec. 2017.
- [26] M. L. Chan, *et al.*, "Design and characterization of MEMS micromotor supported on low friction liquid bearing," *Sensors Actuators, A Phys.*, vol. 177, pp. 1-9, 2012.
- [27] Y. Su, H. Wang, G. Ding, F. Cui, W. Zhang, and W. Chen, "Electroplated hard magnetic material and its application in microelectromechanical systems," *IEEE Trans. Magn.*, vol. 41, no. 12, pp. 4380-4383, 2005.
- [28] N. M. Dempsey, A. Walther, F. May, D. Givord, K. Khlopkov, and O. Gutfleisch, "High performance hard magnetic NdFeB thick films for integration into micro-electro-mechanical systems," *Appl. Phys. Lett.*, vol. 90, no. 9, 2007.
- [29] D. P. Arnold and N. Wang, "Permanent magnets for MEMS," *J. Microelectromechanical Syst.*, vol. 18, no. 6, pp. 1255-1266, 2009.
- [30] E. Diez-Jimenez, J. Esnoz-Larraya, I. Valiente-Blanco, and C. Cristache, "Lubrication free magnetic harmonic drives for harsh space environments," in *Space Robotics Symposium*, 2015.
- [31] "Ansoft Ansys Maxwell v15 - Help assistant." 2018.